Journal of Materials Chemistry C

Diazirine-Based Photo-Crosslinkers for Defect Free Fabrication of Solution Processed Organic Light-Emitting Diodes

Journal:	*Journal of Materials Chemistry C*
Manuscript ID	TC-ART-05-2020-002317.R2
Article Type:	Paper
Date Submitted by the Author:	24-Jul-2020
Complete List of Authors:	DEY, KAUSTAV; Bowling Green State University, Chemistry Chowdhury, Susovan; Bowling Green State University, Chemistry Dykstra, Erik; Iowa State University, Department of Physics and Astronomy Koronatov, Alexander; Bowling Green State University, Chemistry Lu, H.; Bowling Green State University, Chemistry Shinar, Ruth; Iowa State University, Shinar, Joseph; Iowa State University, Physics & Astronomy Anzenbacher, Pavel; Bowling Green State University, Chemistry

Diazirine-Based Photo-Crosslinkers for Defect Free Fabrication of Solution Processed Organic Light-Emitting Diodes

Kaustav Dey,[‡] S. Roy Chowdhury,[‡] Erik Dykstra,[§] Aleksandr Koronatov,[‡] H. Peter Lu,[‡] Ruth Shinar,[†] Joseph Shinar,[§] Pavel Anzenbacher Jr.[‡]*

[‡] Center for Photochemical Sciences, Bowling Green State University, Bowling Green, Ohio 43403.

[§]Ames Laboratory-USDOE and Department of Physics and Astronomy, Iowa State University, Ames, Iowa 50011.

[†]Microelectronics Research Center and Electrical & Computer Engineering Department, Iowa State University, Ames, IA 50011

KEYWORDS: *photopolymerization, cross-linking, diazirine, solution-processed OLEDs, NPB*

ABSTRACT:

The fabrication of solution deposited OLEDs is fraught with difficulties, largely due to the interlayer mixing and surface erosion during sequential deposition of the layers. We demonstrate that these problems can be circumvented by using photopolymerizable diazirine-based cross-linker capable of converting soluble organic materials into highly cross-linked insoluble networks. 3-

trifluoromethyl(aryl)diazirines photolyze readily upon the 10-15 min exposure of 365 nm UV irradiation to generate carbenes, which react with polymers or small molecules via C-H bond insertion producing highly cross-linked materials. This photo-generated cross-linking does not require any catalyst, initiator or short-wavelength UV light and is performed at room temperature, releasing molecular nitrogen as the only byproduct. To show the cross-linked polymer layers do not display inter-layer mixing, we deposited red-emitting regioregular poly(3-hexylthiophene-2,5-diyl) (P3HT) over cross-linked (10% cross-linker) blue emitting dioctyl polyfluorene (PFO) layer. The overlaid layers showed clear and well-defined boundary with no interlayer mixing. The surface morphology of the solution deposited layers was investigated by AFM to show that the cross-linked layers exhibited significant decrease in surface roughness. This is also shown on the example of the hole transporting material 4,4'-bis[N-(1-naphthyl)-N-phenylamino]-biphenyl (NPB) which displayed roughness average to decrease from 6.4 nm to 1.0 nm. The effect of decreased surface roughness on the performance of phosphorescent OLEDs was investigated by fabricating devices with configuration of ITO/PEDOT:PSS/NPB:(0%/5%/10%) cross-linker/MCP:6% $Ir(mppy)_3$/TPBI/CsF/Al. Following the diazirine-mediated cross-linking, the OLEDs displayed a decrease in turn-on voltage from 3.8 V to 3.0 V along with a six-fold enhancement of external quantum efficiency (EQE_{max}) from 1.1% to 6.8% and maximum luminous efficiency increase from 3.8 cd/A to 22.9 cd/A. These results demonstrate that the simple diazirine mediated photo-cross-linking using mild conditions compatible with organic layers is a promising strategy for improving the performance of the solution-processed OLEDs.

1. INTRODUCTION

Solution processing methods for the fabrication of large-area optoelectronic devices are widely sought. In electronic device applications, solution processing methods such as spin coating, blade coating, inkjet, gravure printing, and slot-die coating, to name a few, became the focus of intense research efforts.[1–8] In organic light-emitting diode (OLED) applications, there are two approaches to fabricate multilayer device structures: high-vacuum thermal vacuum evaporation (TVE) and solution processing.[9–12] The desirable way to produce large-area OLEDs is by using solution processing which allows for a significantly lower cost compared to TVE. However, the main challenges for the solution processing technique are the erosion of the previously deposited layer by the solvents used for the next layer deposition, interfacial mixing, or formation of uneven interfaces and surfaces, all of which significantly reduce the device performance. To address this issue, several avenues have been pursued including the polyelectrolyte deposition route,[13,14] the use of “orthogonal solvents”,[15–19] the introduction of a buffer layer,[20,21] electrochemical deposition[22,23] of a buffer layer or the use of organic semiconductors with cross-linkable moieties. This latter approach is particularly promising as it yields insoluble layers with no restrictions for solvents used in the deposition of

subsequent layers. Thus, photo-, thermally, or chemically polymerizable OLED materials have been developed.[24,25] Unfortunately, these approaches suffer from disadvantages that include high temperatures required for cross-linking (e.g. trifluorovinyl-ethers,[26,27] benzocyclobutenes,[28] or styrenes[29,30]), long exposure times required for photo-cross-linking (e.g. cinnamates,[31,32] or acrylates[33,34]), use of photoacid catalysts and two-step curing processes as it is in the case of oxetanes.[35,36] Finally, none of the materials above can be used in a simple and general method. An "additive" cross-linker that could be used to cross-link material regardless of its function is still lacking. Such a cross-linker that could be added at any proportion without detrimental changes in the electronic characteristic of the materials would be a major development in organic electronic devices.

To address this point and also to overcome the above problems, we have developed new cross-linkers based on 3-trifluoromethyl-3-aryldiazirine moieties[37–39] that display several important features: First and foremost, such cross-linkers are able to cross-link virtually any kind of material, whether a small molecule or polymer, regardless

of its function. Secondly, the 3-trifluoromethyl(aryl)diazirines photolyze readily within 10-15 min (at 365 nm UV irradiation) at room temperature while releasing molecular nitrogen as the only byproduct. The diazirine photolysis results in a formation of carbene, which inserts into C-H bonds in its vicinity thereby providing highly cross-linked and insoluble products.[40,41] The reactivity of carbene intermediates is high enough to cross-link C-H bonds of polymers such as dioctyl polyfluorene (PFO) or regioregular poly(3-hexylthiophene-2,5-diyl) (P3HT) as well as small molecules, for example, 4,4'-bis[N-(1-naphthyl)-N-phenylamino]biphenyl (NPB). To study the utility of diazirines in organic electronic devices, we have synthesized two different compounds **1** and **2**. Here, the two diazirine moieties within one molecule make for very effective cross-linking agents (Figure 1).

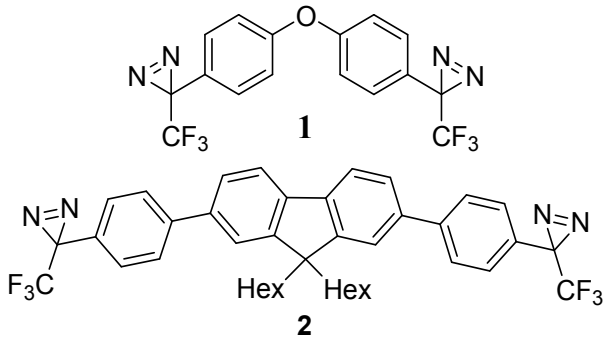

Figure 1. The bis-diazirine cross-linkers **1** and **2** used in this study.

The cross-linking is achieved by the photolysis of the diazirine moiety, which generates a carbene intermediate. Such a carbene intermediate can exist in its singlet or triplet form. The singlet carbene is formed first and reacts with surrounding C-H moieties. However, the carbene singlet can also re-equilibrate to the corresponding triplet and react with a second molecule of carbene or oxygen to produce radical-radical coupling products including the desired heterodimer as well as the undesirable homo-dimer or ketone, respectively.[41,42] Indeed, during the diazirine photolysis in the air-saturated solvents, we have observed traces of the ketone. In the argon-purged solutions, we have observed only the product of the C-H insertion. In the solid-state samples, after 15 minutes cross-linking the IR spectra did not show the characteristic C=O stretching frequency of the corresponding ketone at 1711 cm^{-1} (see Results and Discussion, Figure 6).

The preference for singlet state reactivity is also supported by the literature on the topic.[41] The observed singlet reactivity is a favorable outcome as the formation of carbene dimers or ketones could partially prevent the cross-linking.

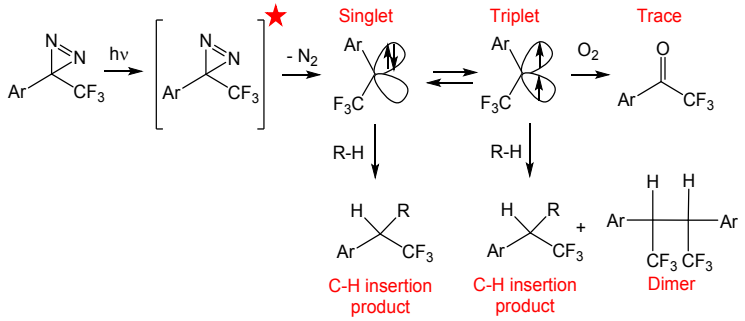

Figure 2. The photolysis of diazirine derivatives and the corresponding products.

Solid-state photolysis experiments were carried out following the procedure briefly outlined in Figure 3. The material to be polymerized was dissolved in a suitable solvent, mixed in various proportions with the cross-linkers **1** or **2** (1-10% by weight) and deposited via spin-coating on a glass slide. The deposited material and cross-linker formed a soluble film, which was subjected to photolysis at room temperature for 5-30 minutes in an ambient atmosphere. This process yields insoluble polymer networks.

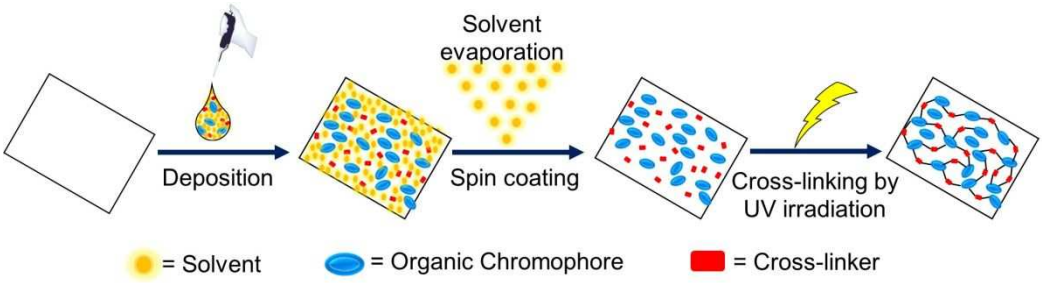

Figure 3. Fabrication of insoluble polymer films using the cross-linkers **1** or **2**.

This process can be used to cross-link polymers such as dioctyl polyfluorene (PFO) or regioregular poly(3-hexylthiophene-2,5-diyl) (P3HT) as well as small molecules, for example, 4,4'-bis[N-(1-naphthyl)-N-phenylamino]biphenyl (NPB), a material commonly used in OLEDs as a hole-transporting and electron-blocking layer (HTL).

2. RESULTS AND DISCUSSION

2.1. Photo-patterning and Fluorescence study:

Under UV irradiation bis-diazirines are very good sources of carbenes that predominantly generate C-H inserted products, converting soluble materials into insoluble highly cross-linked networks. Naturally, this process lends itself to the photolithographic deposition of polymer features. To demonstrate the possibility of photolithographic deposition of two different layers, first PFO with 10% of **2** was photo-patterned to obtain cross-linked PFO (blue) features using a shadow mask (Figure 4).

Here we used 15-minute photolysis using the irradiation with 365 nm UV light (power density 1.8 mW/cm^2) followed by demasking and washing of the patterned glass with THF to remove the unreacted PFO film from under the mask that was not exposed to light. This resulted in the formation of cross-linked emissive PFO (blue) features corresponding to the openings in the shadow mask. Then, P3HT (red) features (Figure 4) were deposited on top of the first blue pixel in such a way that the second pixel of P3HT is partly overlapping with the first (PFO). From the fluorescence image of the overlapped segment it is clear that there is no inter-penetration of the fluorescence emission colors at the intersection of the two polymers in the overlapped region. The two polymer features remain well-defined, despite the sequential solvent deposition and washing.

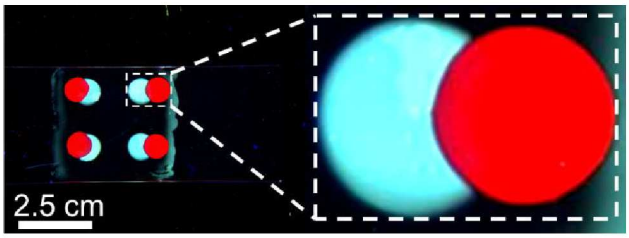

Figure 4. Photolithographic pattern of PFO cross-linked with **2** (10%) (bottom) and P3HT (top), were deposited on top of each other using the shadow-mask photolithography method. The sky-blue color of the PFO layer is due to the presence of green-emitting cross-linker **2** (Fl. Max. 490 nm) and is not due to PFO decomposition. For the emission spectra of PFO with cross-linker **2** (emission max. 490 nm) before and after photolysis see ESI (Figure S4)

To obtain further insight into preventing interfacial mixing of two polymeric layers during sequential deposition of one over another, we made two experiments utilizing polymer bilayers: In the first experiment (Figure 5A), the blue-emitting PFO (λ_{Exc} = 400 nm, λ_{Em} = 435 nm-550 nm, Figure S3A) was drop-cast from a chloroform solution on a quartz glass slide, followed by drying. Then, a thin film of red-emitting P3HT (λ_{Exc} = 560 nm, λ_{Em} = 650 nm-800 nm,

Figure S3B) was drop-cast over the PFO film from a chloroform solution. This resulted in the formation of a blend of the two polymer materials without the formation of a bilayer structure.

In the second experiment (Figure 5B), PFO with 10% of **2** was drop-cast followed by drying. The resulting film was photolyzed by irradiation with 365 nm UV light (power density 1.8 mW/cm^2) for 15 minutes. Then in the similar way a thin film of P3HT was drop-cast over the cross-linked PFO film. In both experiments the excitation spectra (with λ_{Em}^{det} = 700 nm, Figure 5C) and emission spectra (with λ_{Exc} = 400 nm, Figure 5D) were recorded from the side of P3HT at the overlapped region of two polymers. It was observed that the mixed layer lacking the cross-linked PFO exhibits excitation for PFO (300 nm-400 nm), P3HT (500 nm-650 nm) and their complex (400 nm-500 nm). Notably, the incomplete nature of the energy transfer between PFO and P3HT allows for observation of both PFO contribution and P3HT in the samples and enables to distinguish between the uniformly mixed blend (Figure 5A) and the cross-linked bilayer (Figure 5B). Thus, the emission spectra for the same sample displayed features of PFO (400 nm-450 nm), P3HT (600 nm-800 nm) and their complex (400 nm-500 nm). This shows that regardless of sequential deposition of the materials, these formed a homogeneous blend of PFO and P3HT. In the second experiment, where the bilayer with the cross-linked PFO at the bottom was formed and was overlaid with P3HT, the spectra show only the excitation and emission of P3HT at 500 nm-650 nm and at 600 nm-800 nm, respectively. The lack of PFO features in the spectra indicates no mixing of cross-linked PFO with P3HT is taking place as the PFO is effectively separated from the overlaying P3HT layer, and the excitation beam is exclusively absorbed by the P3HT. Together, these data strongly suggest that cross-linking prevents the interfacial mixing of two materials layers, a feature of utmost importance in fabrication of multi-layer devices such as OLEDs.

(A)

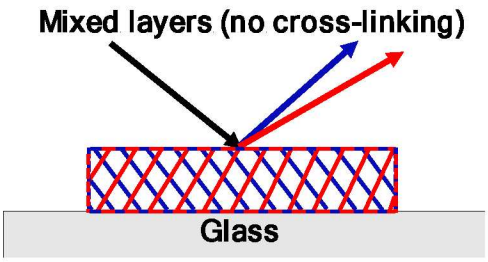

(B)

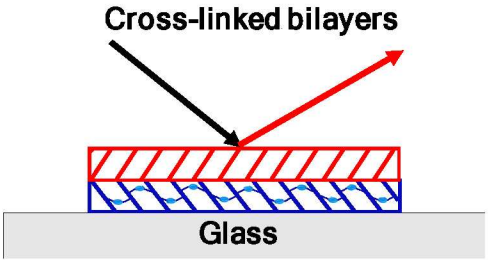

(C) Excitation spectra for λ_{em}^{det} at 700 nm

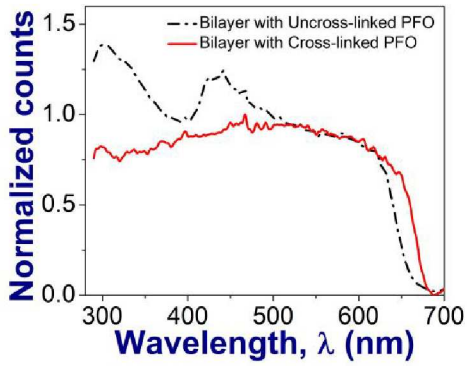

(D) Emission spectra for λ_{ex} at 400 nm

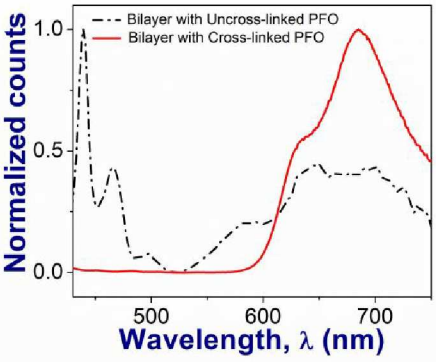

Figure 5. Deposition of P3HT over PFO (A), P3HT over cross-linked PFO (B), excitation spectra of the bilayer for λ_{em}^{det} at 700 nm (C), emission spectra of the bilayer for λ_{exc} at 400 nm (D).

Because of our interest in the solution deposited OLEDs, we decided to study the cross-linking of small molecules such as 4,4'-bis[N-(1-naphthyl)-N-phenylamino]-biphenyl (NPB), a material known as an efficient hole transport and electron blocking material frequently used in OLEDs. Despite the small molecule nature of NPB, insoluble films were realized using the diazirine photolysis and were studied further.

2.2. Cyclic Voltammetry (CV) study:

In order to understand the effect of photolysis and cross-linking on the molecular energy level of NPB, electrochemical properties were studied in thin film using cyclic voltammetry (CV) measurements. The oxidation scans of thin films of photolyzed NPB (0% and 10% **1**) and un-photolyzed NPB were carried out in acetonitrile to estimate the HOMO levels, which were calculated from the onset oxidation potentials of the HOMO levels of ferrocene (-4.8 eV). All films displayed two irreversible oxidation waves and no

reduction wave were detected within the electrochemical window of acetonitrile. Their cyclic voltammograms are shown in Figure S1 and the respective electrochemical data are summarized in Table S1. It was observed that after 30 minutes irradiation with 365 nm UV light (power density 1.8 mW/cm^2) the HOMO-levels of NPB (0% and 10% **1**) were estimated to be -5.43 eV, -5.42 eV, respectively. Similarly, the HOMO level of NPB without the photolysis was found at -5.43 eV. The LUMO levels were estimated to be -2.5 eV for all three samples. Thus, the cyclic voltammetry experiment show that the photolysis as well as cross-linking does not make any change in the molecular energy levels of NPB. This is important because the photolysis does not require that changes be made to device architectures.

2.3. Infra-Red spectroscopy (IR) study:

Figure 6 shows the IR spectra of the un-cross-linked blend of PFO with 10% **2** before (black trace) and after (red trace) cross-linking in the ambient atmosphere, which does not show appreciable band of the characteristic C=O stretching frequency (1711 cm^{-1}). To show how the IR spectrum would have looked like if the ketone C=O was

present, we have recorded a spectrum of a blend of PFO with the precursor **9** (see ESI, Scheme 2, for structure) comprising the carbonyl functional groups. Compound **9** is a precursor for the synthesis of diazirine cross-linked **2** and has been added as an internal standard to acquire the IR spectrum (blue trace).

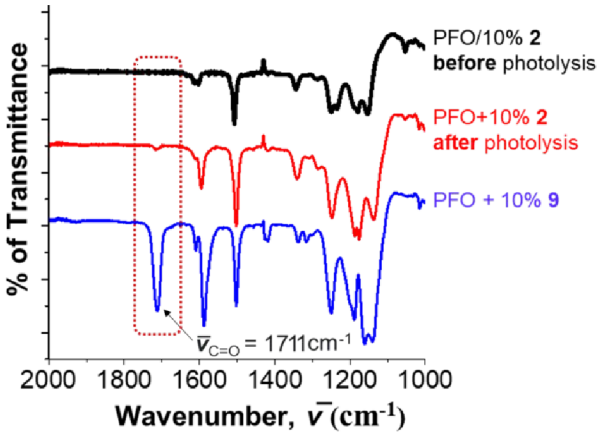

Figure 6. PFO layer photolysis with 10% of cross-linker 2: PFO+10% of cross-linker **2** before (black trace) and after UV-mediated cross-linking (red trace). 10% of carbonyl precursor **9** was added as an internal standard (blue trace).

Similar to the HOMO-LUMO levels that did not show appreciable change due to the cross-linker photolysis, also IR spectra of NPB films (0% and 10% **1**) did not show

any significant changes after 30 minutes of photolysis, suggesting that no structural change affecting the electronic fabric of the NPB is taking place (Figure 7). Similar to Figure 6 recorded for PFO-**2**, the IR spectra for NPB with cross-linker **1** show also a lack of appreciable carbonyl stretching frequency (1712 cm^{-1}). Together, these data suggest that the observed changes in the OLED device performance described in this study are most likely due to the improved morphology of the interfacial layers in the devices rather than changes in the electronic properties of the materials.

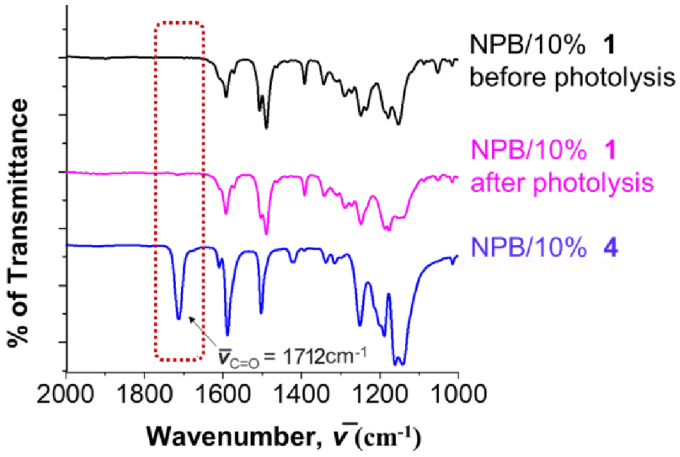

Figure 7. NPB layer photolysis with 10% of cross-linker **1**: NPB+10% of cross-linker **1** before (black trace) and after UV-mediated cross-linking (purple trace). 10% of carbonyl precursor **4** was added as an internal standard (blue trace).

2.4. Atomic Force Microscopy (AFM) study:

Because organic electronic devices such as OLEDs depend on a uniform interface between the layers, we decided to investigate the surface morphology of the deposited (and cross-linked) layers. Toward this end, the effect of cross-linking on surface topography of the deposited films was investigated by AFM, before and after photolysis and finally, also after washing. The solvent washing step mimicked the solution deposition of the next layer of the multi-layer device.

Thus, a 76 nm thick layer of NPB with 10% cross-linker **1** was deposited by spin-coating, and the surface roughness was studied by AFM both before and after photolysis and after washing with THF. Here we used the cross-linker **1** because of its non-emissive nature, which is compatible with NPB. From the topographic images (Figure 8A) of the 20 μm × 20 μm scanned region it was observed that before photolysis the surface was significantly rough. Upon photolysis and washing the surface became significantly smoother. From the surface height profiles (Figure 8B) it was observed that before

photolysis the surface was very rough (the vertical fluctuations of data points were ±8 nm) and became significantly smoother after photolysis (fluctuations of ±3 nm), and after washing it became even smoother with fluctuations of ±1 nm. To investigate the statistical distribution of the vertical fluctuations, fifty different height profiles at different positions of the topographic images were collected and combined to generate the plots where the width of the distribution is proportional to the roughness of the surface (Figure 8C). It was observed that before photolysis the datapoints were broadly distributed between ±12 nm and became significantly narrower with photolysis. After washing the distribution was further reduced to ±3 nm which clearly indicates that cross-linking followed by washing generates smooth surface.

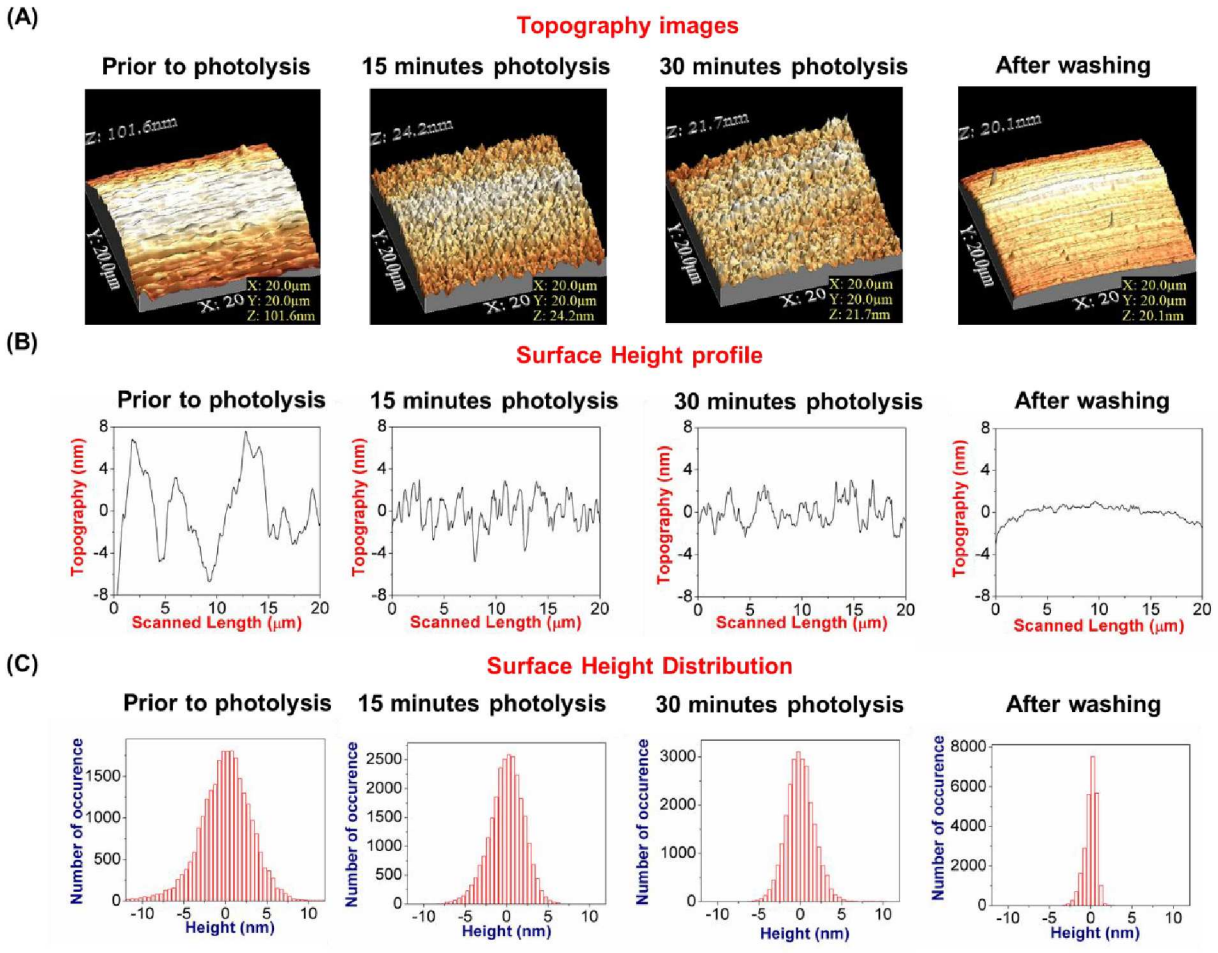

Figure 8. NPB-10% **1** films before and after photolysis, and after washing. Topography images of the 20.0 μm × 20.0 μm section (A). Surface profiles corresponding to the images show the decrease in roughness following the cross-linking and washing (B). Surface height distribution corresponding to the images show the decrease in broadening of the distribution for the photolysis and after washing. (C)

Next the effect of cross-linking was described in terms of roughness average (RA). It was observed that before photolysis the RA was 6.36 nm, which was widely distributed

between 2 nm to 14 nm. After 15 min photolysis the roughness average was reduced to 1.62 nm with narrower distribution between 0.5 nm to 2 nm. After 30 min photolysis the roughness average was further reduced to 1.44 nm. Finally, upon washing with THF the roughness average was decreased to 1.02 nm (Figure 9). The decreased average roughness and the similar roughness distribution for 15 min and 30 min photolysis suggests that after 15 min the NPB surface was fully cross-linked, and the organic layer was not removed by the successive washing with THF.

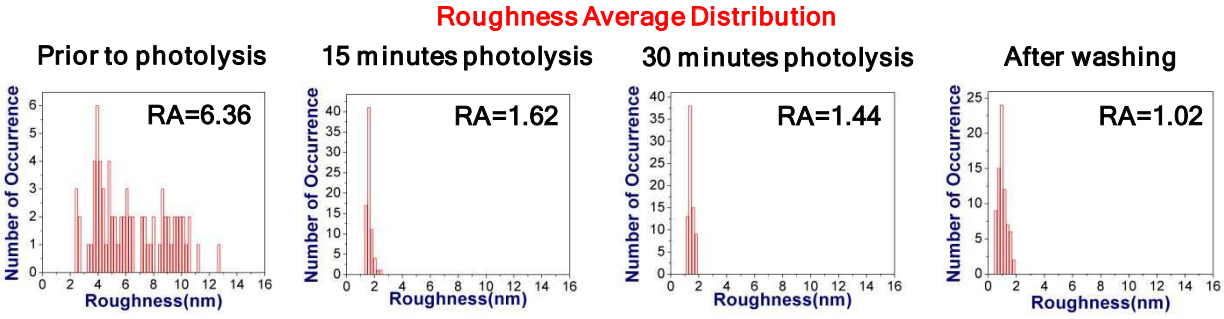

Figure 9. NPB-10% **1** films before and after photolysis, and after washing. The statistical distribution of the surface roughness is narrower following the photolysis demonstrated by the roughness average decrease from 6.36 nm to 1.02 nm.

The dramatic decrease in NPB layer roughness following the cross-linking and washing (which simulates the solution deposition of the subsequent layer in the multi-layer device) inspired us to incorporate the cross-linking step in the fabrication of OLEDs.

2.5. OLED Device Performance:

Smooth layers of uniform thickness of the deposited materials are required for successful operation of the OLEDs. Therefore, the effect of cross-linking on the device performance was studied by fabricating solution-processed OLEDs with the configuration of ITO/ PEDOT:PSS/ NPB:(0%/5%/10%) **1**/ MCP:6% $Ir(mppy)_3$/ TPBI/ CsF/ Al (Figure 10A). This configuration allowed us to study the effect of different amounts of a cross-linker on the device performance. Interestingly, the increasing amount of the cross-linker **1** and the photolysis steps did not diminish the OLED performance. In fact, the cross-linking and the presence of cross-linker residues strongly improved the OLED performance.

All the devices showed uniform and stable emission with a λ_{max} at 511 nm from $Ir(mppy)_3$, with no contribution from NPB, which confirms that charge recombination occurred exclusively in the emissive layer (Figure S2A). Interestingly, when the brightness (cd/m^2) was plotted against voltage (Figure 10B), the turn-on voltage for the devices with no (0%) cross-linker **1**, 5% **1**, and 10% **1** was found to gradually decrease, very significantly, from

3.8 V, 3.03 V, and 3.0 V, respectively. The maximum brightness (Figure 10B), external quantum efficiency (EQE_{max}) (Figure 10C), luminous efficiency (LE_{max}) (Figure 10D), and maximum power efficiency (η_{Pmax}) (Figure S2B) were found to strongly increase with increasing proportion of the cross-linker **1**. The corresponding parameters are shown in Table 1.

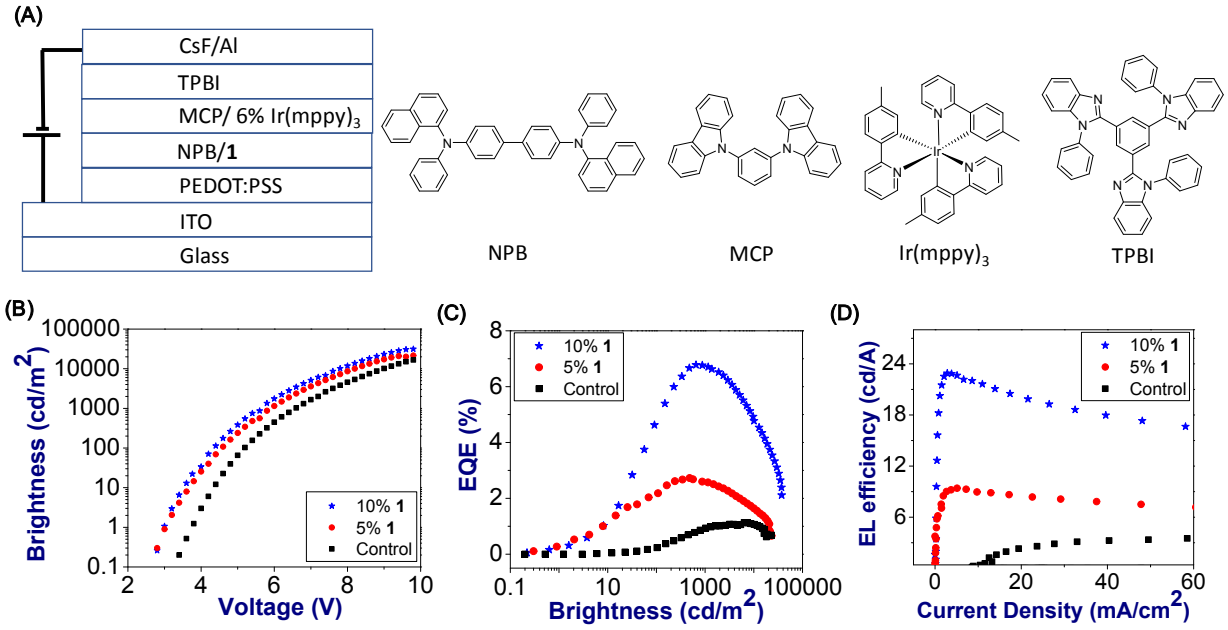

Figure 10. Characterization of the OLEDs comprising various amounts of the cross-linker **1**: Device architecture and chemical structures of the compounds used for device fabrication (A) and comparison of the device characteristics in the solution-processed green OLEDs based on the different amount of **1** in the NPB: Brightness-*vs.*-voltage (B),

maximum external quantum efficiency-brightness (C), maximum electroluminescence efficiency-current density (D).

Table 1. Characteristics of performance of the device parameters.[a)]

HTL	V_{on} (V)	EQE_{max} (%)	B_{max} (cd m^{-2})	LE_{max} (cd A^{-1})	η_{Pmax} (lm W^{-1})
NPB	3.8	1.1	22820	3.8	1.5
NPB + 5% of **1**	3.0	2.7	23130	9.4	5.7
NPB + 10% of	3.0	6.8	37350	22.9	13.1

[a)] All the devices were fabricated and characterized in air and without encapsulation.

It is likely that the UV excitation and the resulting cross-linking followed by washing, which may result in further annealing of the triaryl amine moieties in NPB, leads to conformational relaxation while immobilizing these moieties in a tightly interlocked structure prevents formation of defects.[43] The trends obtained in the tested devices correlate with the AFM experiments for NPB carried out with 10% of cross-linker **1** where it was observed that for the 15 min photolysis the average roughness was reduced from 6.36 nm to 1.62 nm suggesting a decrease in potential aggregation and/or interfacial

defects, which is likely to yield more uniform hole mobility and electron/hole recombination. As a result, we have observed a six-fold improvement in the maximum external quantum efficiency from 1.1% to 6.8% for the devices comprising no **1** to 10% **1**. Furthermore, the device fabricated with 10% of cross-linker **1** exhibited the best performance with maximum luminous efficiency of 22.9 cd/A, maximum brightness of 37,350 cd/m^2, and maximum power efficiency of 13.1 lm/W (Figure S2B). These results are due to cross-linking of the triaryl amine moieties in NPB, immobilizing these in a tightly interlocked structure where the NPB-based tectons**?** are tightly bound closer to one another, providing an effective annealing. This annealing is, we believe, responsible for both better charge transport and improved surface morphology with lower occurrence of defects thereby increasing the device performance.

An additional effect of the crosslinking and annealing is likely the elimination of some defect-induced nonradiative exciton quenching centers. The elimination of these centers might immediately account for the absence of change in the hole mobility, the significant decrease in turn-on voltage, and the sharp increase in the efficiency of the devices. In addition, we believe that the cross-linking and smoothing of the interface between HTL and the emissive layer leads to a decreased degradation of the hole transport layer-emissive layer interface and

a more uniform charge injection and formation of excitons in the emissive layer which in turn leads to sharply improved device performance.

3. Conclusion

In conclusion, we have developed a new method for cross-linking of organic electronic materials utilizing photo-activated diazirine cross-linkers that react with polymers or small molecules to transform soluble organic materials into highly cross-linked insoluble networks. The advantage of the diazirine method is that it appears to be universal in capability to form insoluble layers from all types of materials as long as these possess C-H bonds. Furthermore, it allows for easy-to-achieve photo cross-linking without the presence of any catalyst or initiator while liberating molecular nitrogen as the only side product. Two cross-linkers, each comprising two diazirine moieties were synthesized and tested using shadow-mask photolithography and washing, which allowed for the fabrication of emissive features. AFM was used to study the surface morphology of the cross-linked networks. Prior to cross-linking the materials displayed

significant roughness while after the photolysis the AFM experiments showed dramatically decreased surface roughness, from 6.4 to 1.0 nm, for the hole transporting material NPB.

Fabrication of OLED devices confirmed the utility of the diazirine-based cross-linked networks. Here, for the experimental $Ir(mppy)_3$ OLEDs we observed a decrease in turn-on voltage from 3.8 V for a device fabricated without the cross-linker, to 3.0 V for a device with 10% of the cross-linker. The external quantum efficiency displayed a six-fold enhancement from 1.1% to 6.8%. Similarly, the maximum luminous efficiency increased from 3.8 cd/A to 22.9 cd/A and the maximum power efficiency increased from 1.5 lm/W to 13.1 lm/W. The diazirine-based cross-linking method enables a significant improvement in the OLED performance over any other cross-linking methods reported in the literature. It is suspected that the strongly improved performance is due to relaxation of the NPB network and elimination of some of the nonradiative exciton quenching centers. It is also suspected that the devices' stability improved following the crosslinking process, since that process drastically reduced the devices surface roughness.

Together, the present results demonstrate that the diazirine-based materials can be successfully utilized in the fabrication of emissive features as well as pixels in the experimental OLEDs. We believe that these materials and cross-linking methods may be used for solution fabrication of multi-layer devices such as OLEDs or solar cells.

EXPERIMENAL SECTION

Synthesis of the crosslinkers is described in the Supporting information section.

Sample photolysis and cross-linking:

Photolysis was performed by placing the spin-coated sample 2 cm under Spectroline ENF 280C lamp (power density 1.8 mW/cm^2) with 8W 365 nm output, at a voltage of 115 V, working with a frequency of 60 Hz.

Atomic force microscopy:

All the samples were prepared on a 1cm×1cm sized watch glass. PFO and NPB were spin-coated at 4000 rpm for 30 sec from a 10 mg/ml solution of THF and chloroform respectively and after cross-linking the slides were washed by dipping several times in THF.

Aluminum coated silicon AFM probe (Aspire CT170R-25) was used for topography imaging of the samples. The cantilever force constant was 50 N/m. A full-scale frequency sweep was done to tune the AFM tip and the resonance frequency of the cantilever was found at 170 kHz. The radius of curvature of the tip was 8 nm. The uniform conical shape of the tip fits our requirement to get topography images for measuring surface roughness. Higher Precision closed loop AFM scanning module (PicoSPM, Agilent) was used for imaging. 20×20 μm^2 area of each polymer sample was scanned with a pixel density of 512×512. All AFM data were processed, and roughness was calculated by using WS×M 5.0.

Device Fabrication and General Measurements:

Films were fabricated on 1cm×1cm 20 Ω/square, 140 nm thick ITO-coated glass substrates (Colorado Concept Coatings). The cleaned ITO substrates were treated in UV ozone oven to increase the work function of the ITO and hence facilitate hole injection. The filtered PEDOT:PSS was spin coated at 6000 rpm for 30 s on the ITO to generate a 30 nm layer that was baked in air at 130 °C for 1 hour. Different mixtures (0%, 5%, 10%) of **1** cross-linker and NPB (10 mg/ml) in chloroform were spin-coated at 2000 rpm for 30

s on top of the PEDOT:PSS layer in air and cross-linked by 15 minutes irradiation of 365 nm UV light and then. Then 6% $Ir(mppy)_3$ in MCP were spin coated from a solution of chlorobenzene at 1500 rpm for 30 s in the air and the resulting emitting layer was annealed at 80 °C for 15 minutes in the air and at 80 °C for 15 minutes inside an Ar-filled glove box. Following the annealing step, the films were transferred to a thermal evaporator chamber within the glove box. TPBI, CsF and Al layers were deposited sequentially by thermal evaporation. The thickness of the TPBI layer was 40 nm and that of CsF was 1 nm. The Al cathode was deposited through a shadow mask containing 1.5 mm diameter holes and its thickness was 100 nm. Bias voltages across the OLEDs were supplied by a Kepco DPS 40-2M programmable power supply and the current was measured using a Keithley 2000 multimeter. The OLED's EL was measured by a Minolta LS110 luminance meter and the EL spectra were obtained using an Ocean Optics CHEM2000 spectrometer.

ASSOCIATED CONTENT

Electronic Supporting Information: Methods and materials, Cyclic Voltammetry, Synthesis and characterizations of **1** and **2**.

AUTHOR INFORMATION

Corresponding Author

*E-mail: pavel@bgsu.edu.

Author Contributions

The overall idea of the work was designed by PA. All the works were done by KD. SRC helped in doing the AFM experiments & ED helped in fabrication of the devices. The manuscript was written by KD and PA and all other authors have approved the submission of the manuscript.

Notes

The authors declare no competing financial interest.

ACKNOWLEDGMENT

PA acknowledge support from Bowling Green State University and JS thanks Ames Laboratory which is operated by Iowa State University for the US Department of Energy (USDOE) under Contract No. DE-AC 02-07CH11358. The work at the Ames Laboratory was partially supported by Basic Energy Sciences, Division of Materials Science and Engineering, USDOE.

REFERENCES

1 Y. Khan, A. Thielens, S. Muin, J. Ting, C. Baumbauer and A. C. Arias, *Adv. Mater.*, 2020, **32**, 1905279.

2 X. Che, Y. Li, Y. Qu and S. R. Forrest, *Nat. Energy*, 2018, **3**, 422–427.

3 R. Abbel, I. de Vries, A. Langen, G. Kirchner, H. t'Mannetje, H. Gorter, J. Wilson and P. Groen, *J. Mater. Res.*, 2017, **32**, 2219–2229.

4 T.-W. Koh, A. M. Hiszpanski, M. Sezen, A. Naim, T. Galfsky, A. Trivedi, Y.-L. Loo, V. Menon and B. P. Rand, *Nanoscale*, 2015, **7**, 9140–9146.

5 D. Han, Y. Khan, K. Gopalan, A. Pierre and A. C. Arias, *Adv. Funct. Mater.*, 2018, **28**, 1802986.

6 Y. Khan, F. J. Pavinatto, M. C. Lin, A. Liao, S. L. Swisher, K. Mann, V. Subramanian, M. M. Maharbiz and A. C. Arias, *Adv. Funct. Mater.*, 2016, **26**, 1004–1013.

7 G.-J. N. Wang, F. Molina-Lopez, H. Zhang, J. Xu, H.-C. Wu, J. Lopez, L. Shaw, J. Mun, Q. Zhang, S. Wang, A. Ehrlich and Z. Bao, *Macromolecules*, 2018, **51**, 4976–4985.

8 R. Runser, S. E. Root, D. E. Ober, K. Choudhary, A. X. Chen, C. Dhong, A. D. Urbina and D. J. Lipomi, *Chem. Mater.*, 2019, **31**, 9078–9086.

9 M. Cai, T. Xiao, E. Hellerich, Y. Chen, R. Shinar and J. Shinar, *Adv. Mater.*, 2011, **23**, 3590–3596.

10 E. S. Hellerich, E. Manna, R. Heise, R. Biswas, R. Shinar and J. Shinar, *Org. Electron.*, 2015, **24**, 246–253.

11 E. S. Hellerich, J. J. Intemann, M. Cai, R. Liu, M. D. Ewan, B. C. Tlach, M. Jeffries-EL, R. Shinar and J. Shinar, *J. Mater. Chem. C*, 2013, **1**, 5191.

12 J. J. Intemann, E. S. Hellerich, B. C. Tlach, M. D. Ewan, C. A. Barnes, A. Bhuwalka, M. Cai, J. Shinar, R. Shinar and M. Jeffries-EL, *Macromolecules*, 2012, **45**, 6888–6897.

13 P. K. H. Ho, J.-S. Kim, J. H. Burroughes, H. Becker, S. F. Y. Li, T. M. Brown, F. Cacialli and R. H. Friend, *Nature*, 2000, **404**, 481–484.

14 D. G. Mackanic, W. Michaels, M. Lee, D. Feng, J. Lopez, J. Qin, Y. Cui and Z. Bao, *Adv. Energy Mater.*, 2018, **8**, 1800703.

15 X. Gong, S. Wang, D. Moses, G. C. Bazan and A. J. Heeger, *Adv. Mater.*, 2005, **17**, 2053–2058.

16 W. Ma, P. K. Iyer, X. Gong, B. Liu, D. Moses, G. C. Bazan and A. J. Heeger, *Adv. Mater.*, 2005, **17**, 274–277.

17 F. Huang, L. Hou, H. Wu, X. Wang, H. Shen, W. Cao, W. Yang and Y. Cao, *J. Am. Chem. Soc.*, 2004, **126**, 9845–9853.

18 H. Wu, F. Huang, Y. Mo, W. Yang, D. Wang, J. Peng and Y. Cao, *Adv. Mater.*, 2004, **16**, 1826–1830.

19 A. M. Gaikwad, Y. Khan, A. E. Ostfeld, S. Pandya, S. Abraham and A. C. Arias, *Org. Electron.*, 2016, **30**, 18–29.

20 S.-R. Tseng, S.-C. Lin, H.-F. Meng, H.-H. Liao, C.-H. Yeh, H.-C. Lai, S.-F. Horng and C.-S. Hsu, *Appl. Phys. Lett.*, 2006, **88**, 163501.

21 D. Bilby, B. Frieberg, S. Kramadhati, P. Green and J. Kim, *ACS Appl. Mater. Interfaces*, 2014, **6**, 14964–14974.

22 T. Yu, X. Wu, Y. Lv, L. Liu, L. Du, J. Zhou, Z. Xie and Y. Ma, *J Mater Chem C*, 2014, **2**, 4117–4120.

23 T. Yu, J. Xu, L. Liu, Z. Ren, W. Yang, S. Yan and Y. Ma, *J. Mater. Chem. C*, 2016, **4**, 9509–9515.

24 G. Wantz, L. Derue, O. Dautel, A. Rivaton, P. Hudhomme and C. Dagron-Lartigau, *Polym. Int.*, 2014, **63**, 1346–1361.

25 C. A. Zuniga, S. Barlow and S. R. Marder, *Chem. Mater.*, 2011, **23**, 658–681.

26 J. Ji, S. Narayan-Sarathy, R. H. Neilson, J. D. Oxley, D. A. Babb, N. G. Rondan and D. W. Smith, *Organometallics*, 1998, **17**, 783–785.

27 Y.-H. Niu, M. S. Liu, J.-W. Ka and A. K.-Y. Jen, *Appl. Phys. Lett.*, 2006, **88**, 093505.

28 B. Ma, F. Lauterwasser, L. Deng, C. S. Zonte, B. J. Kim, J. M. J. Fréchet, C. Borek and M. E. Thompson, *Chem. Mater.*, 2007, **19**, 4827–4832.

29 N. Aizawa, Y.-J. Pu, T. Chiba, S. Kawata, H. Sasabe and J. Kido, *Adv. Mater.*, 2014, **26**, 7543–7546.

30 B. Ma, B. J. Kim, D. A. Poulsen, S. J. Pastine and J. M. J. Fréchet, *Adv. Funct. Mater.*, 2009, **19**, 1024–1031.

31 Y. Nakayama and T. Matsuda, *J. Polym. Sci. Part Polym. Chem.*, 1992, **30**, 2451–2457.

32 A. Rehab and N. Salahuddin, *Polymer*, 1999, **40**, 2197–2207.

33 X.-C. Li, T.-M. Yong, J. Grüner, A. B. Holmes, S. C. Moratti, F. Cacialli and R. H. Friend, *Synth. Met.*, 1997, **84**, 437–438.

34 Y.-D. Zhang, R. D. Hreha, G. E. Jabbour, B. Kippelen, N. Peyghambarian and S. R. Marder, *J. Mater. Chem.*, 2002, **12**, 1703–1708.

35 M. S. Bayerl, T. Braig, O. Nuyken, D. C. Müller, M. Groß and K. Meerholz, *Macromol. Rapid Commun.*, 1999, **20**, 224–228.

36 D. C. Müller, T. Braig, H.-G. Nothofer, M. Arnoldi, M. Gross, U. Scherf, O. Nuyken and K. Meerholz, *ChemPhysChem*, 2000, **1**, 207–211.

37 J. Brunner, H. Senn and F. M. Richards, *J. Biol. Chem.*, 1980, **255**, 3313–3318.

38 M. Platz, A. S. Admasu, S. Kwiatkowski, P. J. Crocker, N. Imai and D. S. Watt, *Bioconjug. Chem.*, 1991, **2**, 337–341.

39 J. Wang, N. V. Lebedeva, M. S. Platz and M. D. E. Forbes, *J. Mex. Chem. Soc.*, , DOI:10.29356/jmcs.v53i3.999.

40 G. W. Preston and A. J. Wilson, *Chem. Soc. Rev.*, 2013, **42**, 3289.

41 H. Mehenni, V. Pourcelle, J.-F. Gohy and J. Marchand-Brynaert, *Aust. J. Chem.*, 2012, **65**, 193.

42 A. Admasu, A. D. Gudmundsdóttir, M. S. Platz, D. S. Watt, S. Kwiatkowski and P. J. Crocker, *J. Chem. Soc. Perkin Trans. 2*, 1998, 1093–1100.

43 Z. Ouyang, H. Abrams, R. Bergstone, Q. Li, F. Zhu and D. Li, *Adv. Energy Mater.*, 2020, **10**, 2070014.

TABLE OF CONTENT: